Multiple Lines of Evidence Reveal Rapid, Seasonal Watershed Responses to Enhanced Weathering

Fengchao Sun

fengchao.sun@yale.edu

School of the Environment, Yale University

Robert Rioux

School of the Environment, Yale University

Tim Suhrhoff

Department of Earth and Planetary Sciences, Yale University

Wyatt Tatge

School of the Environment, Yale University

Boriana Kalderon-Asael

Yale University https://orcid.org/0000-0002-5442-8219

Quinn Zacharias

School of the Environment, Yale University

William Miller-Brown

School of the Environment, Yale University

Aaron MacDonald

School of the Environment, Yale University

Esmeralda Garcia

School of the Environment, Yale University

Jamie Shanley

USGS

Peter Raymond

Yale University https://orcid.org/0000-0002-8564-7860

Noah Planavsky

Yale University https://orcid.org/0000-0001-5849-8508

James Saiers

Yale University

Article

Keywords:

Posted Date: December 2nd, 2025

DOI: https://doi.org/10.21203/rs.3.rs-8224816/v1

Additional Declarations: There is **NO** Competing Interest.

Multiple Lines of Evidence Reveal Rapid, Seasonal Watershed Responses to Enhanced Weathering

Fengchao Sun[1,2*], Robert A. Rioux[1,2], Tim Jesper Suhrhoff [2,3], Wyatt Tatge[1,2], Boriana Kalderon-Asael[2,3], Quinn Zacharias[1,2], William A. Miller-Brown[1,2], Aaron A. MacDonald[1,2,4], Esmeralda Garcia[1,2,5], James B. Shanley[6], Peter A. Raymond[1,2], Noah J. Planavsky[2,3], James E. Saiers[1,2]

[1] School of the Environment, Yale University, New Haven, CT, 06511, USA

[2] Yale Center for Natural Carbon Capture, Yale University, New Haven, CT, 06511, USA

[3] Department of Earth and Planetary Sciences, Yale University, New Haven, CT, 06511, USA

[4] Earth and Environmental Science Department, University of Illinois-Chicago, Chicago, IL, 60607, USA

[5] McCormick School of Engineering, Northwestern University, Evanston, IL, 60208, USA

[6] U.S. Geological Survey, New England Water Science Center, Montpelier, VT, 05602, USA

Abstract

Enhanced rock weathering (ERW) is a natural carbon dioxide removal (CDR) approach that captures CO_2 by accelerating silicate weathering using crushed rocks. A major question on the efficacy of ERW is how fast and efficient it is at transporting the products of weathering to drainage networks, and ultimately the ocean. Using a novel whole watershed experiment, we report multiple lines of evidence of rapid and pronounced streamwater chemistry responses within weeks of basalt application (20 t ha^{-1}) to 15% of a 59-ha temperate, headwater catchment. Lines of evidence include an immediate streamwater alkalinity increase of more than 550 μeq L^{-1}, a shift in elemental ratios to silicate endmembers, and a concomitant change in silicon and lithium chemistry reflective of basalt weathering. Finally, our difference-in-differences analysis revealed strong, recurring seasonal ERW treatment effects. ERW contributed 7–17% of observed alkalinity in summer and fall, but much less in winter and spring, reflecting the critical role of the near-surface and stream-proximal zones in alkalinity export, and the effects of precipitation and temperature on ERW rates. Over two years, 9.5–11% of the theoretical CDR potential was exported from the watershed in the form of alkalinity, with an average rate of 34.72 t CO_2 km^{-2} yr^{-1}. This work demonstrates rapid, seasonal watershed responses to ERW and its promise for CDR monitoring, reporting, and verification (MRV), and highlights how climate and hydrological variability set fundamental boundaries on ERW effectiveness across landscapes.

Introduction

Anthropogenic CO_2 emissions are the primary driver of climate change and ocean acidification, profoundly affecting both terrestrial and marine climates and ecosystems.[1, 2] To achieve the Paris Agreement of limiting global warming to less than 2 °C, large-scale carbon dioxide removal (CDR) will be necessary.[3] Terrestrial Enhanced Rock Weathering (ERW) is a promising CDR approach that involves spreading powdered silicate rocks (e.g., basalt) over agricultural and other lands to accelerate chemical weathering reactions that convert atmospheric CO_2 to alkalinity (primarily HCO_3^-) and release base cations.[4, 5] These weathering products may be retained within the watershed or exported with soil waters and groundwaters to streams and rivers that drain into the ocean, where storage lifetimes may exceed tens of millennia.[6, 7] Recent theoretical assessments indicate that ERW implemented on global croplands could sequester 0.5 to 2 Gt CO_2 yr^{-1} at costs comparable to other CDR strategies, which become more competitive when agriculture co-benefits from improved soil health are considered.[8, 9, 10] Despite the growing interest in ERW, uncertainty in its practical potential remains and is underpinned by a scarcity of both observations and demonstrations of approaches suitable for quantifying applied-silicate weathering at the field scale.

Watersheds represent a critical, yet overlooked, unit of analysis for evaluating the efficacy of ERW as a scalable CDR strategy. Watersheds integrate the effects of physicochemical heterogeneity and transient, non-uniform transport processes on the retention, transformation, and export of weathering products.[11] Most ERW estimates rely on feedstock dissolution rates determined in laboratories or in near-surface soils from plot-scale or farm-field experiments.[12, 13, 14] These studies do not capture the suite of watershed processes beneath shallow soil horizons that can alter the timing and magnitude of CDR. For example, ion exchange may delay alkalinity generation as base cations released during silicate dissolution displace adsorbed protons before contributing alkalinity to porewaters,[15] while secondary-clay formation and carbonate precipitation may sequester feedstock weathering products, effectively reducing net CDR.[7, 16, 17] Moreover, the travel times of rainfall and snowmelt through the watershed will lead to hydrologic lags between

feedstock dissolution and the expression of alkalinity in the streamwater signal, a largely unexplored effect with important implications for CDR quantification.

The streamwater chemical response to ERW is likely to be dynamic, shaped by factors that vary at seasonal and sub-seasonal time scales. Seasonal changes in temperature within temperate watersheds hosting ERW deployments will affect weathering rates both abiotically and biotically (through effects on soil pCO_2),[18, 19] while variations in precipitation will modulate watershed wetness and flow path connectivity that, in turn, govern catchment-water residence times and hence the extent of water-feedstock interactions.[20] An understanding of how temperature-precipitation interactions influence temporal variation in ERW contributions to streamwater alkalinity is essential to informing ERW monitoring schemes. It is also crucial to evaluate how downstream processes, such as CO_2 outgassing and carbonate precipitation, will further affect the carbon balance. Yet, the ways these seasonal processes regulate alkalinity generation and export at the watershed scale are largely unknown.

Here we present multiple lines of evidence demonstrating rapid, seasonal watershed responses from ERW, using high-resolution streamwater chemistry data from a 59-ha hay- and pasture-dominated headwater catchment (W-2; average slope ~ 7.3°) within the Sleepers River Research Watershed, Vermont, USA (Fig. 1). Following a one-year baseline monitoring period, we applied Pioneer Valley Basalt powder (hereafter "basalt") in June 2023 over 8.9 ha of the southern portion of the catchment (15% of the total catchment area) at a rate of 20 t ha^{-1}. We isolated the basalt-weathering signal from background water chemistry by analyzing streamwater concentration–discharge (C–Q) relations before and after basalt application and by comparing streamwater observations to a no-basalt counterfactual estimated from WRTDS (Weighted Regressions on Time, Discharge, and Season).[21, 22] We then employed a Generalized Additive Model coupled with a Difference-in-Differences (GAM-DiD) approach[23] that leveraged observations from a nearby reference watershed (W-9) to quantify seasonal dynamics in the streamwater export of basalt-derived alkalinity, base cations and associated CDR rates. Additionally, we applied a novel endmember mixing analysis to evaluate the effects of basalt treatment on seasonal shifts in weathering-

product concentrations within quick-flow and slow-flow pathways that transmit solutes to the stream. This watershed-scale ERW study illuminates how streamwater chemistry responds to the deployment of silicate feedstock and introduces a transferable framework for evaluating the seasonal dynamics of ERW-attributable CO_2 removal.

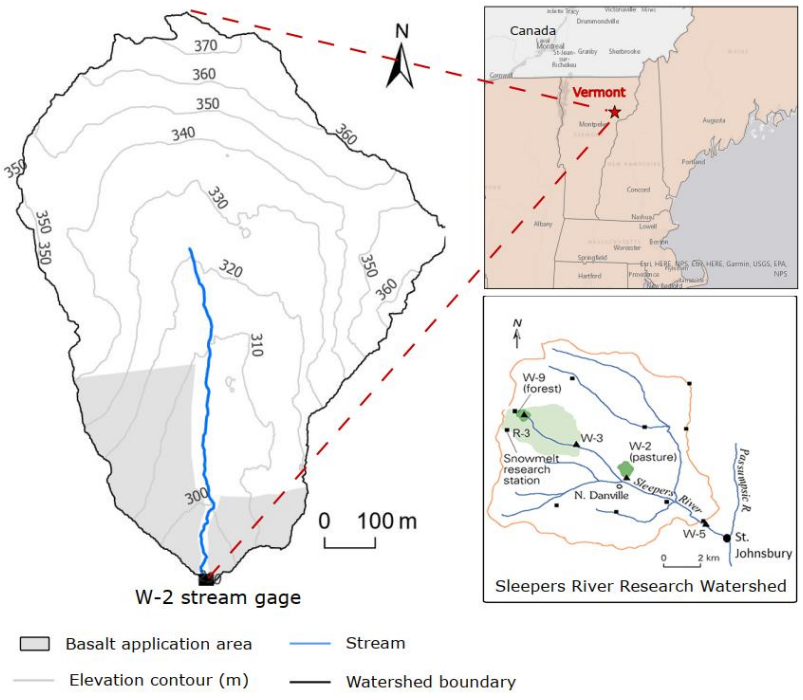

Figure 1. Map of the W-2 watershed study site and basalt application area (grey area) within the Sleepers River Research Watershed (SRRW) in Vermont, USA. The lower inset shows the position of W-2 relative to the W-9 reference watershed in SRRW (modified from Shanley et al.[24]).

Rapid and pronounced streamwater chemistry responses to watershed-scale ERW

Streamwater alkalinity and base cation concentrations in the W-2 stream responded within one month of the basalt application and exhibited sustained elevation relative to counterfactual WRTDS estimates from July to November 2023 (Fig. 2a). In September 2023, measured alkalinity and Ca^{2+} concentrations exceeded counterfactual estimates by more than 550 μeq L^{-1} (Fig. 2b), while measured Mg^{2+} and Na^{+} concentrations exhibited smaller increases (< 35 μeq L^{-1}) relative to the counterfactual (Supplementary Fig. 1). The

absence of similar responses in the W-9 reference watershed underscores that the observed concentration increases in W-2 stream were a direct result of basalt treatment (Fig. 2a, Supplementary Fig. 1). The basalt treatment also affected streamwater concentration-discharge (*C*-*Q*) relations, weakening the pronounced pattern of dilution with increasing flow observed during the baseline (pre-basalt) period for both alkalinity and base cations (Fig. 2c, Supplementary Fig. 2). In addition to concentration increases, elemental ratios of Ca/Na, HCO_3^-/Na, Mg/Na, and Sr/Na shifted toward silicate-weathering endmembers following basalt application (Supplementary Fig. 3), indicating a decline in the relative contribution of carbonate weathering that dominated streamwater composition[25] prior to basalt application.

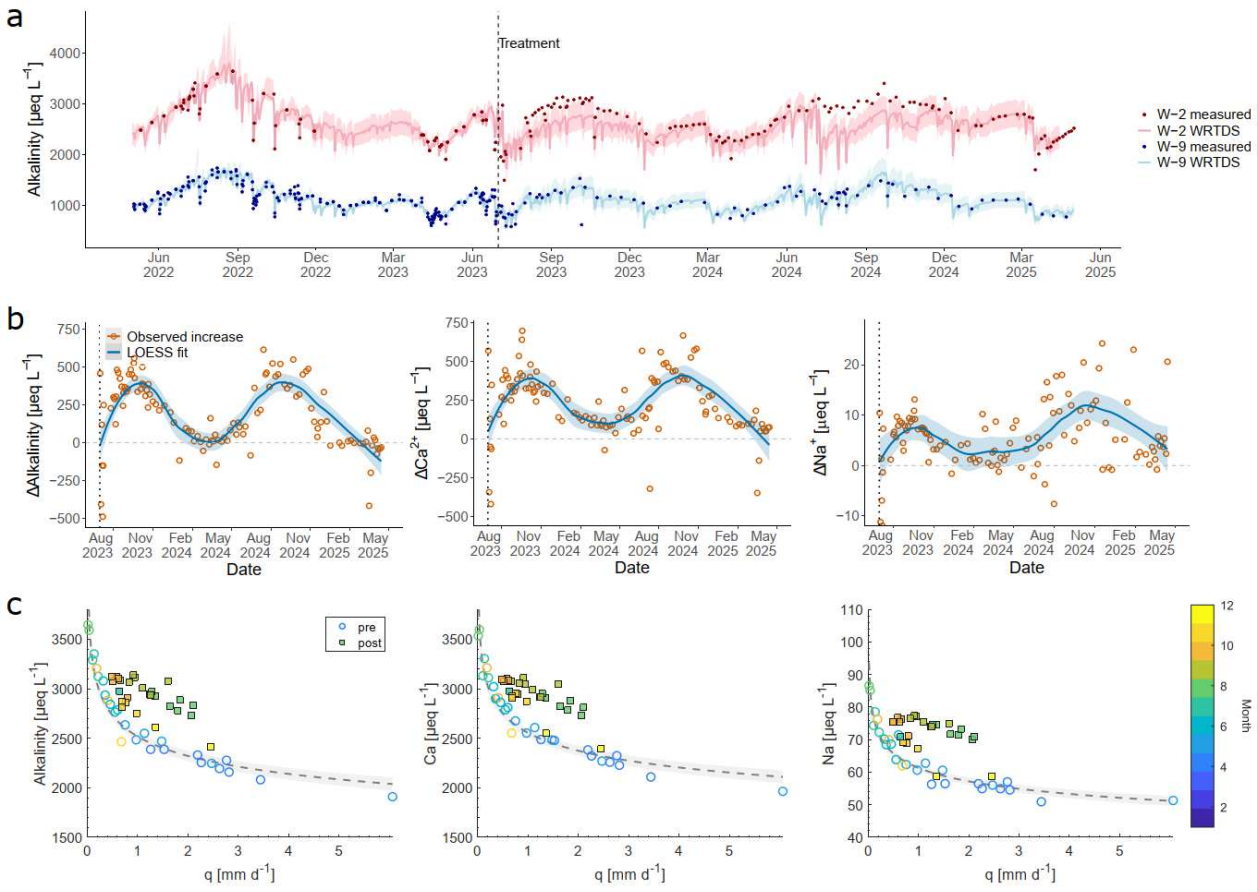

Figure 2. Streamwater concentration changes before and after basalt application. a, Observed and estimated concentrations of alkalinity at W-2 (treatment watershed) and W-9 streams (reference watershed) from May 2022 to April 2025, respectively. The black dashed line separates the pre- and post-basalt application periods. The red and blue lines denote WRTDS-estimated concentrations with shading representing 95% confidence intervals of the

estimates. b, Streamwater concentration changes after basalt application, indicated by the differences between observed concentrations and WRTDS-estimated concentrations for the no-basalt counterfactual (orange circles). Blue lines with shaded areas represent LOESS (Locally Estimated Scatterplot Smoothing) fits with 95% confidence intervals. c, Streamwater concentration-discharge (C-Q) relations at W-2 before basalt application (open circles) and during the first six months after basalt application (solid squares). Data were colored by month of year. Pre-application C-Q data were fitted using a power-law model (grey dashed line) with 95% confidence interval (grey shade). q represents the instantaneous discharge at the time of sample collection.

The post-application enrichment of concentrations of trace metals and silicon provides further evidence for the rapid transport of basalt weathering products to the stream (Supplementary Fig. 2). Concentration increases of silicon and lithium, which are both much more abundant in basalt than carbonates,[26, 27] mirrored the increases in alkalinity and base cations. Moreover, δ^7Li values declined from an average of 19.0 ± 1 ‰ during the pre-treatment period to 17.5 ± 1.0 ‰ within three months after treatment, consistent with increased contributions of isotopically depleted Li derived from basalt-feedstock weathering (basalt δ^7Li value: 2.34 ± 0.65 ‰; Supplementary Fig. 4). Concentrations of rubidium, which substitutes for potassium in feldspars and micas present in the basalt,[28] were similarly greater for equivalent stream discharges under post- relative to pre-treatment conditions. While iron, magnesium, and strontium are released during dissolution of both basalt and carbonates,[29] their concomitant increase with silicon, lithium, and rubidium suggests freshly applied silicates as the most likely source of their increases in concentration immediately following the basalt application (Supplementary Fig. 2).

Preferential streamwater export of Ca, with ERW-driven concentration increases more than 20-fold those of Na and Mg, suggests both enhanced weathering and faster transport of Ca relative to other major cations in response to the basalt treatment (Fig. 2, Supplementary Fig. 2). Transport-related fractionation caused by cation-exchange reactions may potentially contribute to the preferential Ca export. Competitive sorption[30] of cations on the Ca-dominant soil exchange complex at W-2 (mean Ca saturation ~85%[31]) can lower the selectivity of the exchange sites for basalt-derived Ca and lead to the displacement of Ca by other basalt-derived base cations, particularly Mg, resulting in the earlier breakthrough of the less-selectively

bound, Ca-enriched solute relative to Mg. In addition, some Mg released from basalt may be retained in Mg-rich clays;[32] however, this sink appears minor given the absence of ^{7}Li enrichment in streamwater after treatment (Supplementary Fig. 4). Furthermore, incongruent dissolution of abundant basalt minerals, particularly clinopyroxene, promotes Ca release over Mg,[33] while plagioclase dissolution favors Ca over Na and proceeds more rapidly than Si loss.[34] Together, competitive sorption on the Ca-dominant soil exchange complex and selective mineral dissolution may act synergistically to enhance calcium export.

Seasonality of the ERW treatment effect

The ERW-attributable streamwater signal exhibited recurring seasonal patterns during the two years following basalt application, with stronger responses in summer and fall and weaker responses in winter and spring (Fig. 3a–c). The GAM-DiD model revealed that the basalt treatment produced statistically significant changes in streamwater chemistry during July–September 2023, with ERW accounting for 14% to 18% of alkalinity, Ca, Mg, Na, and Si (Δc %; Fig. 3a–c and Supplementary Fig. 5a). This strong treatment effect, coinciding with high discharge during summer storms (Fig. 3g, h), drove elevated ERW-sourced export (i.e., solute load per watershed area) in summer, which then declined as streamflow decreased later in the season (Fig. 3d–f). The ERW treatment effect on concentration remained significant but weakened from October–December 2023 (Fig. 3a–c), and stream discharge also trended downward during this period (Figure 3g), leading to more than a 50% reduction in the export of alkalinity, base cations, and Si (Fig. 3d-f, Table 1). During the wintertime (January–March 2025) when stream flow and temperature were at their lowest (Fig 3g, i), ERW treatment effects on solute concentrations were the weakest and insignificant, and loads decreased sharply, with ERW-sourced alkalinity export falling from its summertime high of 102.55 t CO_2 km^{-2} yr^{-1} to less than 3 t CO_2 km^{-2} yr^{-1} and base cations showing approximately proportional decreases (Fig. 3d–f, Table 1). The treatment effect on streamwater concentration increased again in April–June 2024 as temperatures rose and streamwater export was controlled by snowmelt-driven discharge (Fig. 3a–f). Comparable seasonal patterns in the ERW-attributable concentration and export percentages were observed during the second year (July 2024–April 2025), though with slightly lower intensities (Fig. 3a–f, Table 1).

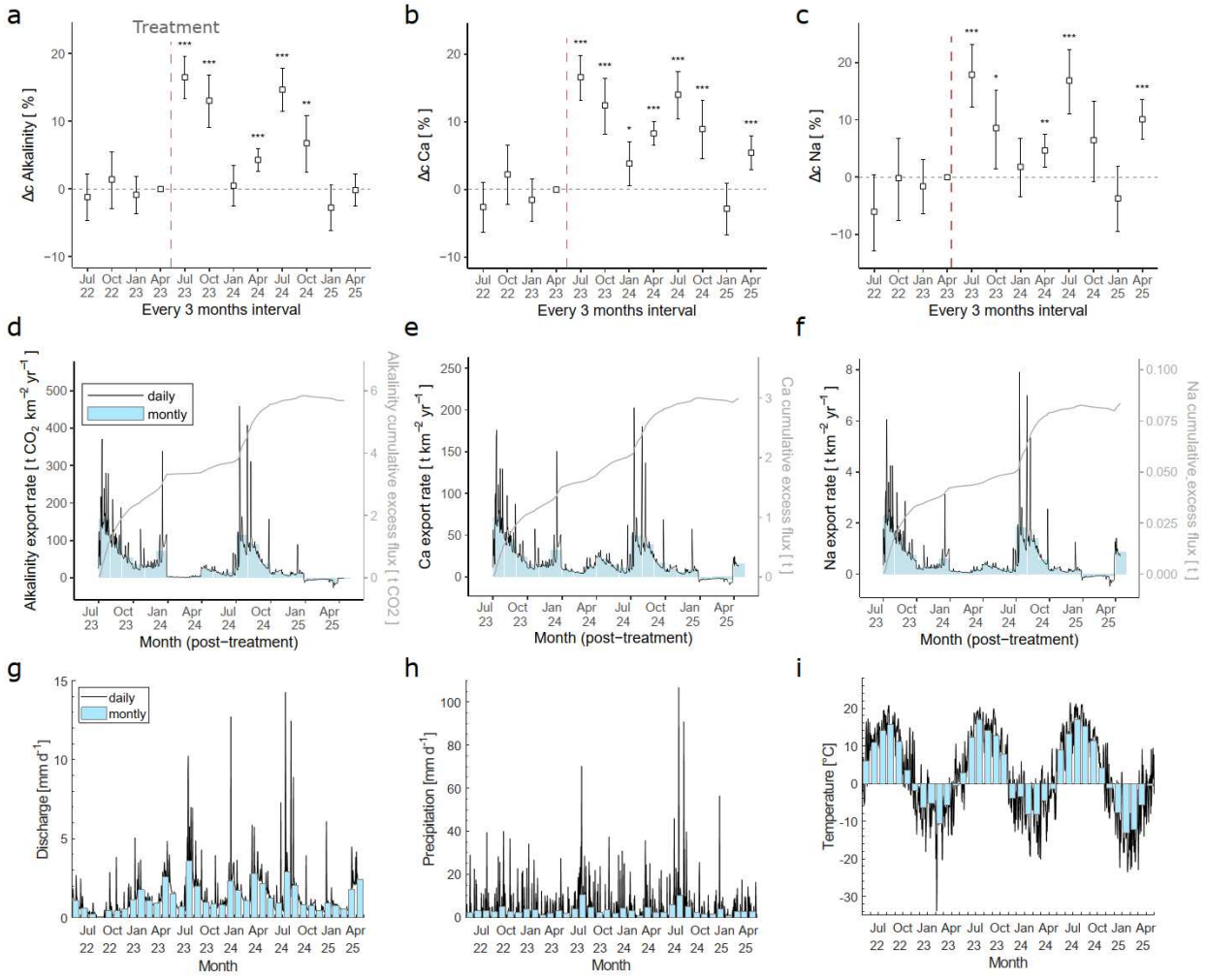

Figure 3. Temporal dynamics of the ERW treatment effects, solute export rates, and hydroclimatic variables. a–c, ERW-attributable concentration change (Δc %) estimated from the GAM-DiD analysis. Significance levels are indicated as follows: *** $p \leq 0.001$, ** $p \leq 0.01$, * $p \leq 0.05$, · $p \leq 0.1$, and not significant ($p > 0.1$). The red dashed line separates the pre- and post-basalt application periods. d–f, Daily (solid black line) and monthly average (blue bar) export rates of the basalt weathering products. Gray solid lines represent the cumulative export flux of the basalt weathering products. g–i, Time series of daily (black lines) and monthly average (blue bars) discharge, precipitation, and temperature).

Table 1 Export estimation of basalt weathering products with 95% confidence intervals.

	Alkalinity as CO_2 [t CO_2 km^{-2} yr^{-1}]	Ca [t km^{-2} yr^{-1}]	Na [t km^{-2} yr^{-1}]	Mg [t km^{-2} yr^{-1}]	Si [t km^{-2} yr^{-1}]
Jul– Sep 2023	102.55 (86.53, 117.30)	47.20 (39.27, 54.45)	1.50 (1.11, 1.84)	1.41 (1.09, 1.71)	2.83 (2.09, 3.53)
Oct– Dec 2023	46.18 (33.76, 57.46)	20.41 (14.21, 26.01)	0.39 (0.08, 0.66)	0.53 (0.26, 0.77)	0.87 (0.35, 1.36)
Jan– Mar 2024	2.87 (-12.27, 17.12)	8.98 (1.60, 15.86)	0.12 (-0.21, 0.41)	0.14 (-0.16, 0.42)	0.66 (0.11, 1.19)
Apr – Jun 2024	17.18 (10.97, 23.17)	15.21 (12.15, 18.14)	0.25 (0.11, 0.38)	0.37 (0.26, 0.49)	0.41 (0.17, 0.66)
Jul – Sep 2024	80.59 (65.00, 94.93)	35.05 (27.26, 42.18)	1.29 (0.90, 1.61)	1.19 (0.90, 1.45)	2.51 (1.82, 3.18)
Oct – Dec 2024	12.37 (4.55, 19.52)	7.88 (4.10, 11.30)	0.16 (-0.03, 0.32)	0.34 (0.20, 0.47)	0.58 (0.28, 0.86)
Jan– Mar 2025	-6.84 (-15.90, 1.66)	-2.71 (-6.93, 1.21)	-0.09 (-0.25, 0.06)	0.12 (-0.07, 0.31)	0.28 (-0.07, 0.61)
Apr 2025	-0.92 (-14.93, 12.44)	15.47 (8.55, 22.03)	0.88 (0.60, 1.13)	0.68 (0.43, 0.92)	1.06 (0.49, 1.62)
Annual mean	34.72 (30.39, 39.05)	18.71 (16.58, 20.83)	0.53 (0.44, 0.63)	0.59 (0.50, 0.68)	1.16 (0.97, 1.34)

This recurring seasonal cycle suggests that interactions among rainfall-runoff processes, watershed wetness, and temperature shaped the seasonal patterns in ERW-derived solute concentrations and export. Comparison of *C*-*Q* relations in the summer-fall periods before and after basalt application reveals a weakening of the streamwater dilution pattern, which is consistent with a lowering of the difference in solute concentrations within slow-flow and quick flow pathways that deliver water and solutes to the stream (Fig. 4a, Supplementary Fig. 7). In contrast, the *C*-*Q* relations for winter-spring periods exhibited greater slopes and were similar before and after basalt application (Fig. 4a, Supplementary Fig. 7), which suggests comparatively large differences in solute concentrations between quick- and slow-flow pathways in the baseline period were preserved after the basalt treatment. Seasonal *C*-*Q* relations fitted with a sigmoidal inverse power-law model (equation (6), with quick-/slow-flow endmembers) show that solute concentrations associated with slow-flow pathways remained stable year-round (alkalinity: 4186 ± 228 μeq L^{-1}, Ca: 4256 ± 455 μeq L^{-1}); however, concentrations of solutes transmitted via quick-flow pathways increased markedly during the summer-fall seasons of the post-application period with alkalinity and Ca increasing by up to 1200 μeq L^{-1} (Fig. 4b, Supplementary Fig. 7).

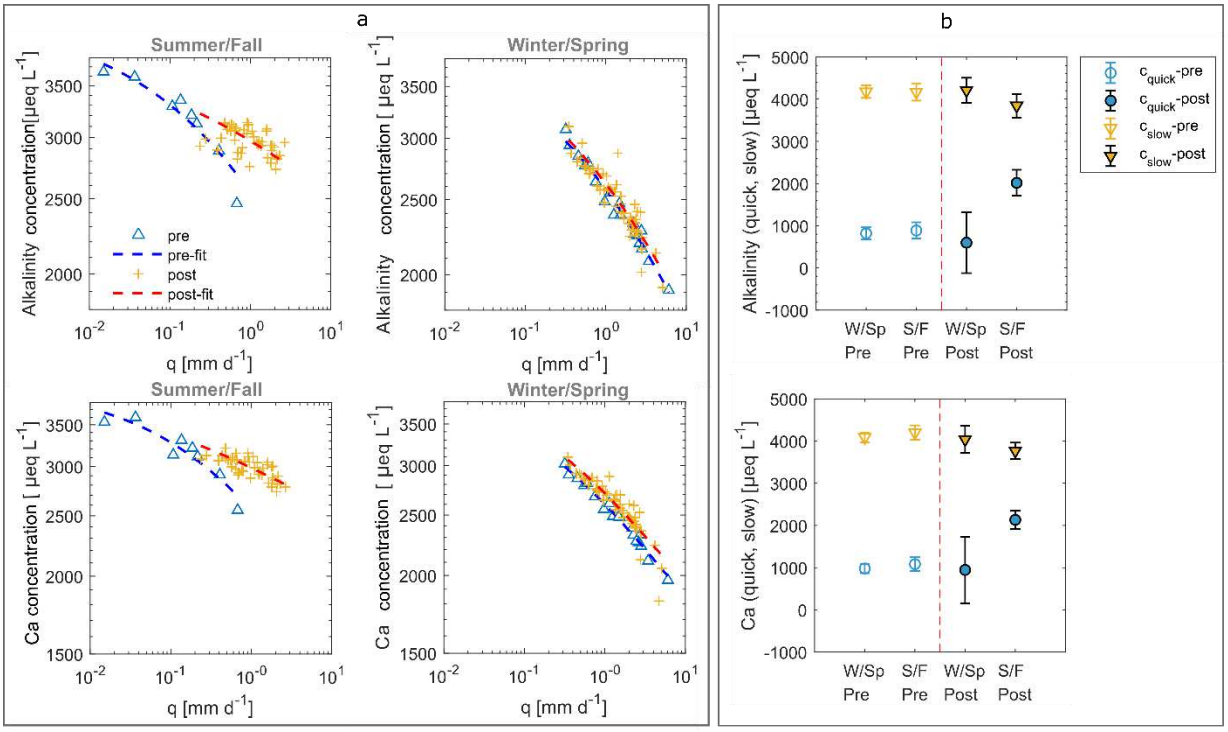

Figure 4. Seasonal concentration-discharge (*C*-*Q*) relations and estimated concentrations of slow-/quick-flow endmembers pre- and post-basalt application. a, Observed *C*-*Q* relations for alkalinity and Ca for summer/fall and winter/spring periods prior to (blue triangles) and after basalt application (orange crosses) and corresponding model fits (dashed lines). b, Alkalinity and Ca concentrations of quick-flow (blue) and slow-flow (orange) endmembers for winter/spring and summer/fall periods prior to (open symbols) and after basalt application (filled symbols) as estimated from inversion of equations (4)–(6).

The pronounced summer-fall response of quick-flow pathways to the basalt treatment highlights the role of near-surface and stream-proximal zones in controlling seasonal ERW solute export. In temperate catchments, quick flow comprises both new water (recent rainfall or snowmelt) that is delivered to the stream via overland and near-surface flow and resident (pre-event) soil water and shallow groundwater that is displaced primarily during hydrologic events and in diminishing quantities during recession to baseflow.[24, 35] ERW-derived solutes in quick flow are likely associated with shallow pre-event water that has interacted extensively with the feedstock between storm periods, with comparatively minor inputs from feedstock interactions with new water. Lowland areas proximal to the stream, with a shallow water table

and high soil moisture, act as key sources of such solute-rich quick flow. In contrast, slow flow showed no detectable ERW signals, reflecting its upslope origin toward the watershed divide and correspondingly long residence times. Additionally, silicate dissolution rates are highly temperature-dependent,[36] increasing exponentially with warming,[36, 37] and further influenced by soil pCO_2 levels, which rise with temperature due to enhanced microbial and root respiration. This temperature effect, then, likely underpins the increase in ERW solute concentrations in summer-fall quick flow (Fig. 4b), while the suppressed winter-spring ERW response reflects both lower temperatures and the strong dilution effect from snowmelt-driven quick flow.

Export rates of basalt weathering products and associated carbon dioxide removal

Our study demonstrates efficient export of basalt weathering products in the first two years following ERW. On an annual basis, ERW-derived alkalinity export averaged 9.47 t C km^{-2} yr^{-1}, equivalent to 34.72 t CO_2 km^{-2} yr^{-1} (Table 1), which is among the highest observed rates compared to other studies that quantify CDR via changes in alkalinity (and/or cation) fluxes in streams, leachate water, or pore waters.[32, 38, 39, 40, 41, 42] Previous watershed-scale studies reported 2.5–13 t CO_2 km^{-2} over 15 years after wollastonite addition (30 t ha^{-1}) in a temperate forest, [38] while another study reported an average of 0.001 t CO_2 km^{-2} across three small watersheds (<0.02 km^{-2}) within a tropical oil palm plantation after three annual applications of basalt (50 t ha^{-1}).[39] Lysimeter and mesocosm studies usually yield lower rates (1–26 t CO_2 km^{-2} yr^{-1}), even though many used higher rock application rates of up to 100 t ha^{-1}.[12, 40, 41, 42, 43] The lack of leachate ERW signals in some of these experimental studies likely reflects a combination of factors, including short experimental durations, the absence of natural structure and associated transport pathways in repacked soils, and the use of acidic soils that may scavenge base cations and neutralize alkalinity.

Over 22 months, the ERW-derived alkalinity export was 63.8 t CO_2 km^{-2} (5.7 t over the 8.9 ha treated area, Fig. 3d), representing approximately 11% of the maximum CDR potential of the applied basalt (582 t CO_2 km^{-2}, 51.8 t CO_2 over the 8.9 ha treated area, equation (1)). While the applied basalt contained minor inorganic carbon (~0.14%, or 0.22 t in total), its maximum dissolution would account for only 14%

of the exported alkalinity from ERW. This indicates that most of the alkalinity export was generated through silicate weathering, corresponding conservatively to 9.5% of the basalt's CDR potential. This value approaches the upper limit of realizable export as predicted by reactive-transport models that account for cation sorption and secondary mineral formation; under such constraints, alkalinity export is generally estimated to be < 10% after two years in most areas of the U.S.[44] One likely reason for relatively more efficient solute transport in this study (9.5 – 11%) is likely that initial base saturation of soils in W-2 was high (85% Ca), indicating that the potential maximum loss to cation sorption may be lower compared to U.S. averages, as well as suitable climatic and hydrological conditions. Collectively, these findings demonstrate that weathering products can be exported efficiently at the catchment scale over seasonal-to-annual hydrologic timescales that govern their transport to streams and rivers.

Implications for ERW applications at watershed scale

This study demonstrates that watersheds can serve as a natural integrator of ERW signals, providing a promising, scalable unit for MRV (monitoring, reporting, and verification) by capturing the combined effects of basalt weathering rates, hydrological transport, and climatic variability (e.g., temperature and precipitation) on the exports of ERW-derived alkalinity and base cations. In contrast to laboratory studies and field trials,[45, 46] the ERW treatment effects estimated by the watershed approach (with GAM-DiD) showed distinct, recurring seasonal patterns, with broadly comparable intensities in both years when comparing the same seasons, despite a slight overall decrease in the second year. This temporal consistency suggests that comparable hydrological and environmental conditions in 2023 and 2024 (Fig. 3g–i) exerted a stronger control on the weathering signal than processes intrinsic to the weathering material itself, such as the depletion of reactive surface area or secondary phase formation, at the timescale of about two years.[45, 47] Therefore, CDR efficiency of large-scale ERW may be more dynamic and sustainable than inferred from laboratory kinetics alone.

The breakthrough time of the ERW signal in the W-2 streamwater between basalt application and the initial stream response was rapid, on the order of weeks, whereas 9.5–11% of the potential maximum

CDR has been exported as alkalinity over the experimental period of two years. Given the heterogeneity of soils and aquifers in the watershed,[48] with variable flow paths and water residence times (with mean residence time of 1.3 years at W-2[49]), it is likely that weathering products transported via slow-flow path have yet to emerge and/or are diluted beyond detection. Our stable water isotope analysis showed that 23 ± 2% of streamflow comprises water younger than 2.3 ± 0.8 months, implying that most water resides in longer-term catchment storage. Thus, while our observations capture the leading edge of ERW signals, they also point to the potential for delayed and distributed responses over longer timescales. Uptake by vegetation[50] and retention on soil exchange sites[15, 38] may further postpone the export of ERW products by keeping them in the upper soil layers before they reach deeper horizons or streamwater. Capturing the full carbon removal potential of ERW will therefore require integrated catchment monitoring strategies that account for both short-term hydrologic pulses and longer-term stream and groundwater transport, especially under changing conditions driven by climate change. Comprehensive baseline monitoring with control catchments provides the strongest basis for attributing the effects of ERW.

Furthermore, the climate- and hydrology-driven seasonal shifts in weathering and solute transport rates indicate that ERW potential may vary across regions and climates. In cold climates, low soil temperatures and pCO_2 constrain weathering kinetics, while in arid systems, low soil moisture and limited runoff may restrict the weathering and export of ERW products.[41] By contrast, catchments with pronounced seasonal precipitation, such as humid temperate and tropical regions, are more likely to sustain both high weathering rates and efficient solute export if CEC is low. These linkages highlight how climate and hydrological variability set fundamental boundaries on the effectiveness of ERW across landscapes. Future watershed-scale ERW research across diverse regions and climates is needed to better understand the factors affecting ERW weathering rates, carbon transport pathways, and its environmental impacts.

Methods

Site description

The study site, the W-2 watershed, is a 59-ha headwater catchment situated within the Sleepers River Research Watershed in Danville, Vermont, USA. It is a low-elevation (285 m to 377 m) agricultural catchment, with 27% forest and 73% hayfield and pasture.[51] The area experiences a cold, humid continental climate, with mean annual precipitation of 1,050 mm yr^{-1} and mean annual air temperature of 5.7 °C. The mean daily discharge from the W-2 stream averages 0.76 ± 0.19 mm d^{-1}, with approximately two-thirds of annual discharge occurring as baseflow.[25] While runoff peaks in spring during snowmelt, heavy storms during summer and fall may drive discharge to levels more than an order-of-magnitude above baseflow. The stream weir location for discharge measurement, where water samples were also collected, is Lat: 44.45958 Lon: -72.0920.

The watershed is underlain by fine, silty calcareous till deposited during the Wisconsinan glaciation.[52] Beneath the till is the Lower Devonian and Upper Silurian Waits River Formation, which consists of quartz–mica schist with beds of calcareous granulite.[51] Till thickness ranges from less than 2 m near the hilltops to over 10 m downslope towards the stream. The soil in the upland hayfield is a sandy loam, whereas the downslope pasture soil is a loam with approximately equal sand and silt contents, with pH ranging from 4.9 to 7.7 (median pH 6.1).[31]

Basalt application and characteristics

We applied Pioneer Valley Basalt powder at a rate of 20 t ha^{-1} to an 8.9-ha area of hayfield and pasture in the southern portion of the W-2 watershed (Fig. 1) in June 2023. The basalt feedstock was sourced from metamorphosed basaltic rock from the Holyoke Range, Massachusetts USA (Rock Dust Local, Bridport, Vermont, USA). The moisture content of basalt powder was 10.1 ± 0.2% at the time of application. Modal mineralogy (thin-section point counts) of the basalt was 35.1% clinopyroxene, 33.7% plagioclase, 10.6% sericite, 9.2% chlorite, 6.7% actinolite, 3.8% opaque minerals, and 0.9% quartz. The basalt feedstock consisted primarily of SiO_2 (51.6%), Al_2O_3 (13.6%), and Fe_2O_3 (13.2%), with notable contents of CaO (9.2%), MgO (5.8%), and Na_2O (2.98%) (Supplementary Table 1). Based on this oxide content, the estimated stoichiometry of the basalt is $Ca_{0.36}Mg_{0.31}Na_{0.209}Fe_{0.36}Si_{1.87}Al_{0.58}O_6$ (molar mass of 211 g mol^{-1}).

The total inorganic carbon content was 0.14 ± 0.02%, measured on the Eltra CS Analyzer. The p80 value (80% of the particles have a diameter less than or equal to) of the basalt powder equaled 297 μm. The Brunauer–Emmett–Teller (BET) specific surface area of the basalt was 4.3 m^2 g^{-1}, measured using the BET N_2-adsorption method on an Anton Paar Nova 800.

The CDR potential [t CO_2 km^{-2}] of the basalt was calculated by using the following equation:

$$CDR_{potential} = \sum_{\substack{i= \\ Ca,Mg,Na}} n_i \cdot \frac{M_{CO_2}}{M_{basalt}} \cdot R_{app} \cdot (1 - \Theta) \qquad \text{equation (1)}$$

where n_i [eq] is the charge equivalent of each major cation (i.e., Ca, Mg, and Na) in basalt ($Ca_{0.36}Mg_{0.31}Na_{0.209}Fe_{0.36}Si_{1.87}Al_{0.58}O_6$); M_{CO_2} [g mol^{-1}] and M_{basalt} [g mol^{-1}] is the molar mass of CO_2 and basalt, respectively; Θ [%] is the moisture content of basalt; and R_{app} [t km^{-2}] is the basalt application rate.

Streamwater chemistry and meteorological observations

Streamwater samples were collected biweekly or monthly before basalt application from May 2022 to June 2023, and twice per week after basalt application from July 2023 to April 2025, with more intensive sampling during storms (hourly). The collected streamwater samples were either filtered onsite immediately or filtered in the lab within 24 h through 0.22 μm syringe filters, and divided into subsamples in acid-washed, filtered-streamwater-rinsed, high-density polyethylene (HDPE) bottles for major cations [calcium (Ca^{2+}), magnesium (Mg^{2+}), sodium (Na^+), potassium (K^+)], alkalinity, and trace metal analysis. The samples for trace metal analysis were acidified by adding 50% nitric acid. All the samples were stored at 4 °C until analysis. All measurements were performed at the Yale Analytical and Stable Isotope Center (YASIC) following the methods described in ref.[25] Aliquots from selected samples were further processed for Li separation and measurements at the Yale Geochemistry Center. The samples were first digested with aqua regia, evaporated and redissolved in 1 ml of 0.2N HCl, and then Li was separated following the methods described in ref.[53] The Li isotopic composition measurements were performed on a Thermo Finnigan Neptune Plus ICP-MS and the Li isotopic compositions are reported relative to the L-SVEC-1 lithium

carbonate standard, NIST 8545. A typical standard error of a single measurement was 0.07 ‰ (1σ) and the external precision was better than 0.08 ‰ (1STD).

In addition to our own observations, we used published measurements of stream chemistry made from March 1992 to May 2017 at W-2 watershed, as well as published measurements of stream discharge and chemistry made from January 2019 to April 2025 at W-9 watershed from the U.S. Geological Survey (USGS) aqueous chemistry database of the Sleepers River Research Watershed, Danville, Vermont.[54] Watershed W-9 is a 41-ha forested headwater catchment located 6 km from W-2 in the Sleepers River Research Watershed. Daily estimates of air temperature and precipitation for the W-2 and W-9 watersheds were extracted from the Parameter-elevation Regressions on Independent Slopes Model (PRISM) database.[55]

Estimating streamwater chemistry for a no-basalt counterfactual with WRTDS

We applied WRTDS to estimate streamwater chemistry at the W-2 watershed for a counterfactual scenario representing conditions without the basalt application. The model was trained on long-term data (March 1992 – June 2023), and the calibrated model was used with W-2 daily discharge measurements made between July 2023 and April 2024 as one means to estimate how streamwater solute concentrations at W-2 would vary during the post-treatment period in the absence of the basalt application. The WRTDS method was implemented using the EGRET R package.[21] Briefly, the daily streamwater solute concentrations were simulated in WRTDS as

$$ln(c) = \beta_0 + \beta_1 \ln(q) + \beta_2 t + \beta_3 \sin(2\pi t) + \beta_4 \cos(2\pi t) + \varepsilon \quad \text{equation (2)}$$

where c is the estimated concentration (μeq L^{-1}), β_i are the regression coefficients, q is the daily mean discharge ($m^3\ s^{-1}$), t is time in decimal years, and ε is the unexplained variation. This method uses a weighted regression, where the relevance of each observation to the estimation point is defined by the distance in time, season, and discharge between the observation and the estimation point, thereby generating a unique set of parameters for every combination of q and t values.[21, 22]

Estimation of basalt treatment effect using a Difference-in-Differences approach

To quantify basalt-treatment effects on streamwater chemistry, we implemented a Generalized Additive Model coupled with a Difference-in-Differences (GAM-DiD) approach that leverages stream chemistry observations from a reference watershed. Watershed W-9 was chosen as the reference owing to its similar climate and parallel hydrological and hydrochemical responses relative to W-2 (Fig. 1). The model structure is as follows:

$$\log c_i = \beta_0 + s_1(\log Q_i) + s_2(PPT_i) + s_3(T_i) + s_4(Month_i, by = Watershed_i) + \beta_1 \cdot Watershed_i + \beta_2 \cdot Prepost_i + \beta_3 \cdot (Watershed_i \times Prepost_i) + \varepsilon_i \quad \text{equation (3)}$$

where $\log c_i$ is the response variable (log-transformed solute concentration c_i [μeq L^{-1}] for sample i) from either the treatment or the reference watershed; s_1, s_2, s_3, and s_4 are the spline-based smooth functions used to model nonlinear relationships between each predictor and $\log c_i$; $\log Q_i$ is the log transformed discharge Q_i [mm d^{-1}]; PPT_i [mm d^{-1}] is the precipitation; T_i [°C] is the daily average air temperature; $(Month_i, by = Watershed_i)$ indicates the month effect by watershed (treatment or reference); $Watershed_i$ is the binary indicator for treatment and reference watershed (0 = reference, 1 = treatment); $Prepost$ is a categorical indicator for pre- and post-treatment period, where -3, -2, -1, and 0 correspond to the pre-treatment period (three-month intervals from May 2022 to June 2023), and 1–8 represent post-treatment periods (three-month intervals, except for April 2025, which covers one month due to the absence of W-9 water chemistry records thereafter); $Watershed \times Prepost$ is the interaction term representing the core DiD contrast that captures the difference in differences (post vs. pre) between treatment and reference watersheds. Fixed effects comprise an intercept β_0 (expected log concentration in the baseline pre-treatment period for the reference watershed at reference covariate levels), a watershed indicator β_1 (time-invariant treatment-reference difference at baseline), period ("Prepost") indicators β_2 (shifts common to both watersheds for each period relative to baseline), and the $Watershed \times Prepost$ interactions β_3, which quantify the difference-in-differences for each period. The variable ε_i is the residual error.

The coefficients are on the log scale, so exponentiation yields multiplicative effects on concentration. Of particular importance is the quantity $(exp(\beta_3) - 1)/ (exp(\beta_3) \times 100$, which gives the

366 percentage of streamwater concentration attributable to ERW; we denote this as Δc [%]. This estimated
367 treatment effect from the GAM-DiD model was used to calculate the export rate of the basalt weathering
368 products through stream runoff. The GAM-DiD model was implemented using the mgcv package in R.

369 To enable a DiD analysis despite the mismatched sampling dates of two watersheds, we used the
370 WRTDS model to estimate daily solute concentrations for the reference watershed (W-9). The WRTDS
371 model was trained using W-9 data from January 2019 to June 2023, and the daily estimates that
372 corresponded to times of measurements at W-2 were used as reference watershed concentrations in the DiD
373 analysis.

374 **Endmember mixing analysis**

375 To trace basalt-derived solutes and quantify flow path contributions to the W-2 stream, we developed a
376 quick-flow/slow-flow mixing model with sigmoidal inverse power-law function (equations (4)–(6)). Here,
377 we define two flow-path endmembers of streamwater composition: one is slow-flow water comprised
378 primarily of deeper groundwaters with longer residence times and the second is quick-flow water comprised
379 of near-surface and overland-flow waters with shorter residence times. Quick-flow/slow-flow separation
380 has been used with analysis of stream concentration-discharge relations to infer flow paths by which water
381 is transported through the watershed.[56, 57] A non-linear relation between stream discharge q and the slow-
382 and quick-flow fractions (i.e., f_{slow} and f_{quick}) can be derived under the assumption that f_{slow} decreases
383 with q and asymptotically approaches zero as q approaches infinity and that the sum of f_{slow} and f_{quick}
384 always equals unity (equation (4), Supplementary Fig. 6a). We combined this sigmoidal inverse power-law
385 function with an endmember mixing equation (equation (5)) to estimate a relation between stream discharge
386 and stream concentration (equation (6)), such that

$$f_{slow} = \frac{1}{1 + a_{slow} \cdot q^{b_{slow}}} \qquad \text{equation (4)}$$

$$c_{stream} = c_{slow} \cdot f_{slow} + c_{quick} \cdot (1 - f_{slow}) \qquad \text{equation (5)}$$

$$c_{stream} = (c_{slow} - c_{quick}) \cdot \left(\frac{1}{1 + a_{slow} \cdot q^{b_{slow}}}\right) + c_{quick} \quad \text{equation (6)}$$

where f_{slow} [-] is the fractional contribution of slow-flow water to streamflow, q [mm d^{-1}] is discharge of the stream, a_{slow} [-] and b_{slow} [-] are fitted values to identify the f_{slow} change with q in the watershed. c_{stream} [μeq L^{-1}] is the streamwater concentration, c_{slow} [μeq L^{-1}] is the slow-flow endmember concentration, and c_{quick} [μeq L^{-1}] is the quick-flow endmember concentration.

By fitting equations (4)–(6) to streamwater chemistry data for the pre-treatment period (January 2008 – May 2017 and May 2022 – June 2023), we estimated the endmember concentrations of c_{quick} and c_{slow} of the solutes (i.e., Ca, Mg, Na, and alkalinity) together with the parameters a_{slow} and b_{slow} (Supplementary Fig. 6). With the estimated values of a_{slow} and b_{slow} from the pre-treatment data, we then estimated c_{quick} and c_{slow} of each solute after basalt application. This analysis provides a way to explore whether basalt weathering signals (e.g., elevated alkalinity and Ca concentration) in the stream are more closely associated with quick-flow or slow-flow pathways, and how such signals may evolve after basalt treatment. While we do not assume that the relation between flow pathways and discharge is precise or universally transferable across catchments or time periods, this approach serves as an illustrative tool to shed light on the potential origins of observed streamwater concentration changes. The model fitting was performed in MATLAB R2023b, using the *fmincon* for pre-treatment nonlinear parameter estimation and *isqlin* for post-treatment endmember estimation.

Quantifying the young water fraction of streamflow

We calculated the young water fraction (F_{yw}) of the W-2 streamflow using $\delta^{18}O$ isotope values from precipitation and streamwater from March 1992 to June 2011 (USGS aqueous chemistry database),[54] following a published approach.[58] In the following equation, F_{yw} is defined as the proportion of the transit-time distribution younger than a threshold age and can be estimated from the ratio of the amplitudes of

tracer signals (e.g., $\delta^{18}O$ isotope) in streamwater and precipitation for gamma functions with shape parameter α between 0.2 and 2:[58]

$$F_{yw} = A_s/A_p \quad \text{equation (7)}$$

where A_s [-] and A_p [-] are the amplitudes of the $\delta^{18}O$ signals in streamwater and precipitation, respectively.

The amplitude and phase of the seasonal $\delta^{18}O$ from precipitation and streamwater were estimated by nonlinear fitting of

$$c(t) = A\sin(2\pi ft - \varphi) + k \quad \text{equation (8)}$$

where, A [-] is the amplitude, f [year^{-1}] is the frequency, t [year] is time, φ [-] is the phase shift, and k [-] is the vertical shift.

The calculated gamma shape parameter α for the W-2 transit time distribution is 0.81, estimated by solving equation (9) using Newton's method:

$$\varphi_s - \varphi_p = \alpha \arctan\sqrt{\left(\frac{A_s}{A_p}\right)^{-\frac{2}{\alpha}} - 1} \quad \text{equation (9)}$$

where φ_s [-] and φ_p [-] are the phase shifts for streamwater and precipitation, respectively, With the calculated α at W-2 falling within the range of 0.2–2, we reported F_{yw} of the W-2 streamflow as the fraction of water younger than 2.3 ± 0.8 months.[58] Gaussian error propagation was used to estimate uncertainties.

References

1. Lee H, Calvin K, Dasgupta D, Krinner G, Mukherji A, Thorne P*, et al.* IPCC, 2023: Climate change 2023: Synthesis report, summary for policymakers. Contribution of working groups i, II and III to the sixth assessment report of the intergovernmental panel on climate change [core writing team, h. Lee and j. Romero (eds.)]. IPCC, geneva, Switzerland. 2023.

2. Köhler P, Hartmann J, Wolf-Gladrow DA. Geoengineering potential of artificially enhanced silicate weathering of olivine. *Proceedings of the National Academy of Sciences* 2010, **107**(47)**:** 20228-20233.

3. Shukla PR, Skea J, Slade R, Al Khourdajie A, van Diemen R, McCollum D*, et al.* Climate change 2022: Mitigation of climate change. *Contribution of working group III to the sixth assessment report of the Intergovernmental Panel on Climate Change* 2022, **10:** 9781009157926.

4. Hartmann J, West AJ, Renforth P, Köhler P, De La Rocha CL, Wolf-Gladrow DA*, et al.* Enhanced chemical weathering as a geoengineering strategy to reduce atmospheric carbon dioxide, supply nutrients, and mitigate ocean acidification. *Reviews of Geophysics* 2013, **51**(2)**:** 113-149.

5. Strefler J, Amann T, Bauer N, Kriegler E, Hartmann J. Potential and costs of carbon dioxide removal by enhanced weathering of rocks. *Environmental Research Letters* 2018, **13**(3)**:** 034010.

6. Taylor LL, Quirk J, Thorley RMS, Kharecha PA, Hansen J, Ridgwell A*, et al.* Enhanced weathering strategies for stabilizing climate and averting ocean acidification. *Nature Climate Change* 2016, **6**(4)**:** 402-406.

7. Harrington KJ, Hilton RG, Henderson GM. Implications of the Riverine Response to Enhanced Weathering for CO2 removal in the UK. *Applied Geochemistry* 2023, **152:** 105643.

8. Beerling DJ, Kantzas EP, Lomas MR, Wade P, Eufrasio RM, Renforth P*, et al.* Potential for large-scale CO 2 removal via enhanced rock weathering with croplands. *Nature* 2020, **583**(7815)**:** 242-248.

9. Beerling DJ, Leake JR, Long SP, Scholes JD, Ton J, Nelson PN*, et al.* Farming with crops and rocks to address global climate, food and soil security. *Nature Plants* 2018, **4**(3)**:** 138-147.

10. Baek SH, Kanzaki Y, Lora JM, Planavsky N, Reinhard CT, Zhang S. Impact of Climate on the Global Capacity for Enhanced Rock Weathering on Croplands. *Earth's Future* 2023, **11**(8)**:** e2023EF003698.

11. Bormann FH, Likens GE. Nutrient Cycling. *Science* 1967, **155**(3761)**:** 424-429.

12. Holzer IO, Nocco MA, Houlton BZ. Direct evidence for atmospheric carbon dioxide removal via enhanced weathering in cropland soil. *Environmental Research Communications* 2023, **5**(10)**:** 101004.

13. Renforth P, von Strandmann PP, Henderson G. The dissolution of olivine added to soil: Implications for enhanced weathering. *Applied Geochemistry* 2015, **61:** 109-118.

14. Dietzen C, Rosing MT. Quantification of CO2 uptake by enhanced weathering of silicate minerals applied to acidic soils. *International Journal of Greenhouse Gas Control* 2023, **125:** 103872.

15. Johnson CE, Driscoll CT, Blum JD, Fahey TJ, Battles JJ. Soil chemical dynamics after calcium silicate addition to a northern hardwood forest. *Soil Science Society of America Journal* 2014, **78**(4)**:** 1458-1468.

16. Strandmann P, He XQ, Zhou Y, Wilson DJ. Comparing open versus closed system weathering experiments using lithium isotopes. *APPLIED GEOCHEMISTRY* 2025, **189**.

17. Maher K, Steefel CI, White AF, Stonestrom DA. The role of reaction affinity and secondary minerals in regulating chemical weathering rates at the Santa Cruz Soil Chronosequence, California. *Geochimica et Cosmochimica Acta* 2009, **73**(10)**:** 2804-2831.

18. Gaillardet J, Dupré B, Louvat P, Allegre C. Global silicate weathering and CO2 consumption rates deduced from the chemistry of large rivers. *Chemical geology* 1999, **159**(1-4)**:** 3-30.

19. Deng K, Yang S, Guo Y. A global temperature control of silicate weathering intensity. *Nature Communications* 2022, **13**(1)**:** 1781.

20. Maher K. The dependence of chemical weathering rates on fluid residence time. *Earth and Planetary Science Letters* 2010, **294**(1)**:** 101-110.

21. Hirsch RM, De Cicco LA. User guide to exploration and graphics for RivEr Trends (EGRET) and dataRetrieval: R packages for hydrologic data: US Geological Survey; 2015. Report No.: 2328-7055.

22. Hirsch RM, Moyer DL, Archfield SA. Weighted regressions on time, discharge, and season (WRTDS), with an application to Chesapeake Bay river inputs. *JAWRA Journal of the American Water Resources Association* 2010, **46**(5)**:** 857-880.

23. Tazhitdinova A, Vazquez-Bare G. Difference-in-Differences with Unequal Baseline Treatment Status: National Bureau of Economic Research; 2023.

24. Shanley JB, Chalmers AT, Denner JC, Clark SF, Sebestyen SD, Matt S*, et al.* Hydrology and biogeochemistry datasets from Sleepers River Research Watershed, Danville, Vermont, USA. *Hydrological Processes* 2022, **36**(2).

25. Sun F, Rioux RA, Miller-Brown WA, Shrestha B, Shanley JB, Planavsky NJ*, et al.* Long-term trends of streamwater chemistry in an agricultural watershed: Effects of anthropogenic and climatic factors. *Science of The Total Environment* 2025, **970:** 179017.

26. Hoefs J, Sywall M. Lithium isotope composition of quaternary and tertiary biogene carbonates and a global lithium isotope balance. *Geochimica et Cosmochimica Acta* 1997, **61**(13)**:** 2679-2690.

27. Hathorne EC, James RH. Temporal record of lithium in seawater: A tracer for silicate weathering? *Earth and Planetary Science Letters* 2006, **246**(3)**:** 393-406.

28. Simmons EC. rubidiumRubidium: Element and geochemistry. *Geochemistry*. Springer Netherlands: Dordrecht, 1998, pp 555-556.

29. Gaillardet J, Viers J, Dupré B. 7.7 - Trace Elements in River Waters. In: Holland HD, Turekian KK (eds). *Treatise on Geochemistry (Second Edition)*. Elsevier: Oxford, 2014, pp 195-235.

30. Violante A. Chapter Three - Elucidating Mechanisms of Competitive Sorption at the Mineral/Water Interface. In: Sparks DL (ed). *Advances in Agronomy*, vol. 118. Academic Press, 2013, pp 111-176.

31. Zacharias Q, Rioux R, Sun F, Tatge W, Pihlap E, Nyavor E*, et al.* Spatiotemporal soil fertility responses to an enhanced rock weathering deployment within a temperate, agricultural watershed. *Preprint at https://doiorg/1070212/cdrxiv2025460v1 (2025)*.

32. Niron H, Vienne A, Frings P, Poetra R, Vicca S. Exploring the synergy of enhanced weathering and Bacillus subtilis: A promising strategy for sustainable agriculture. *Global Change Biology* 2024, **30**(9)**:** e17511.

33. Schott J, Berner RA, Sjöberg EL. Mechanism of pyroxene and amphibole weathering—I. Experimental studies of iron-free minerals. *Geochimica et Cosmochimica Acta* 1981, **45**(11)**:** 2123-2135.

34. Peters SC, Blum JD, Driscoll CT, Likens GE. Dissolution of wollastonite during the experimental manipulation of Hubbard Brook Watershed 1. *Biogeochemistry* 2004, **67**(3)**:** 309-329.

35. Saiers JE, Fair JH, Shanley JB, Hosen J, Matt S, Ryan KA*, et al.* Evaluating Streamwater Dissolved Organic Carbon Dynamics in Context of Variable Flowpath Contributions With a Tracer-Based Mixing Model. *Water Resources Research* 2021, **57**(10)**:** e2021WR030529.

36. Dessert C, Dupré B, Gaillardet J, François LM, Allègre CJ. Basalt weathering laws and the impact of basalt weathering on the global carbon cycle. *Chemical Geology* 2003, **202**(3-4)**:** 257-273.

37. Kump LR, Brantley SL, Arthur MA. Chemical weathering, atmospheric CO2, and climate. *Annual Review of Earth and Planetary Sciences* 2000, **28**(1)**:** 611-667.

38. Taylor LL, Driscoll CT, Groffman PM, Rau GH, Blum JD, Beerling DJ. Increased carbon capture by a silicate-treated forested watershed affected by acid deposition. *Biogeosciences* 2021, **18**(1)**:** 169-188.

39. Larkin CS, Andrews MG, Pearce CR, Yeong KL, Beerling DJ, Bellamy J*, et al.* Quantification of CO2 removal in a large-scale enhanced weathering field trial on an oil palm plantation in Sabah, Malaysia. *Frontiers in Climate* 2022, **4:** 959229.

40. Holden FJ, Davies K, Bird MI, Hume R, Green H, Beerling DJ*, et al.* In-field carbon dioxide removal via weathering of crushed basalt applied to acidic tropical agricultural soil. *Science of The Total Environment* 2024, **955:** 176568.

41. Buckingham FL, Henderson GM, Holdship P, Renforth P. Soil core study indicates limited CO2 removal by enhanced weathering in dry croplands in the UK. *Applied Geochemistry* 2022, **147:** 105482.

42. Amann T, Hartmann J, Struyf E, de Oliveira Garcia W, Fischer EK, Janssens I*, et al.* Enhanced Weathering and related element fluxes – a cropland mesocosm approach. *Biogeosciences* 2020, **17**(1)**:** 103-119.

43. Vienne A, Frings P, Rijnders J, Suhrhoff TJ, Reershemius T, Poetra RP*, et al.* Weathering without inorganic CDR revealed through cation tracing. *EGUsphere* 2025, **2025:** 1-24.

44. Kanzaki Y, Planavsky N, Zhang S, Jordan J, Suhrhoff TJ, Reinhard C. Soil cation storage is a key control on the carbon removal dynamics of enhanced weathering. *Environmental Research Letters* 2025, **20**(7)**:** 074055.

45. White AF, Schulz MS, Lawrence CR, Vivit DV, Stonestrom DA. Long-term flow-through column experiments and their relevance to natural granitoid weathering rates. *Geochimica et Cosmochimica Acta* 2017, **202:** 190-214.

46. White AF, Brantley SL. The effect of time on the weathering of silicate minerals: why do weathering rates differ in the laboratory and field? *Chemical Geology* 2003, **202**(3)**:** 479-506.

47. Calabrese S, Wild B, Bertagni MB, Bourg IC, White C, Aburto F*, et al.* Nano- to Global-Scale Uncertainties in Terrestrial Enhanced Weathering. *Environmental Science & Technology* 2022, **56**(22)**:** 15261-15272.

48. Molins S, Svyatsky D, Xu Z, Coon ET, Moulton JD. A multicomponent reactive transport model for integrated surface-subsurface hydrology problems. *Water Resources Research* 2022, **58**(8)**:** e2022WR032074.

49. Shanley JB, Sebestyen SD, McDonnell JJ, McGlynn BL, Dunne T. Water's Way at Sleepers River watershed – revisiting flow generation in a post-glacial landscape, Vermont USA. *Hydrological Processes* 2015, **29**(16)**:** 3447-3459.

50. Dalmora AC, Ramos CG, Silva Oliveira ML, Silva Oliveira LF, Homrich Schneider IA, Kautzmann RM. Application of andesite rock as a clean source of fertilizer for eucalyptus crop: Evidence of sustainability. *Journal of Cleaner Production* 2020, **256:** 120432.

51. Shanley JB, Kendall C, Smith TE, Wolock DM, McDonnell JJ. Controls on old and new water contributions to stream flow at some nested catchments in Vermont, USA. *Hydrological Processes* 2002, **16**(3)**:** 589-609.

52. Wright SF. Late Wisconsinan ice sheet flow across northern and central Vermont, USA. *Quaternary Science Reviews* 2015, **129:** 216-228.

53. Kalderon-Asael B, Katchinoff JAR, Planavsky NJ, Hood AvS, Dellinger M, Bellefroid EJ*, et al.* A lithium-isotope perspective on the evolution of carbon and silicon cycles. *Nature* 2021, **595**(7867)**:** 394-398.

54. Matt S, Shanley J, Chalmers A, Sebestyen S, Merriam J, Bailey S. Aqueous chemistry database, sleepers river research watershed, Danville, Vermont, 1991-2018. *US Geological Survey data release https://doiorg/105066/P9380HQG* (2021).

55. PRISM CG. Oregon State University, https://prism.oregonstate.edu, data created 1 May 2025, accessed 1 May 2025.

56. Westfall TG, Peterson TJ, Lintern A, Western AW. Slow and Quick Flow Models Explain the Temporal Dynamics of Daily Salinity in Streams. *Water Resources Research* 2025, **61**(6)**:** e2024WR039103.

57. Minaudo C, Dupas R, Gascuel-Odoux C, Roubeix V, Danis P-A, Moatar F. Seasonal and event-based concentration-discharge relationships to identify catchment controls on nutrient export regimes. *Advances in Water Resources* 2019, **131:** 103379.

58. Kirchner JW. Aggregation in environmental systems – Part 1: Seasonal tracer cycles quantify young water fractions, but not mean transit times, in spatially heterogeneous catchments. *Hydrol Earth Syst Sci* 2016, **20**(1)**:** 279-297.

Ethics declarations

The authors declare that they have no competing interests.

Acknowledgments

We thank Brad Erkkila and Jonas Karosas from Yale Analytical and Stable Isotope Center (YASIC) for their help in the measurements of water samples. We also acknowledge the graciousness of Dave Langmaid, who enabled our access to the W-2 watershed. This work was supported by the Yale Center for Natural Carbon

642 Capture (YCNCC). Any use of trade, firm, or product names is for descriptive purposes only and does not
643 imply endorsement by the U.S. Government.

Supplementary Files

This is a list of supplementary files associated with this preprint. Click to download.

- SI251126final.docx